

# Nonlinear wavelength selection in surface faceting under electromigration

Fatima Barakat, Kirsten Martens, and Olivier Pierre-Louis  
*Laboratoire de Physique de la Matière Condensée et Nanostructures,  
Université Lyon 1, 43 Bd du 11 novembre,  
69622 Villeurbanne, France.*

(Dated: June 15, 2021)

We report on the control of the faceting of crystal surfaces by means of surface electromigration. When electromigration reinforces the faceting instability, we find perpetual coarsening with a wavelength increasing as  $t^{1/2}$ . For strongly stabilizing electromigration, the surface is stable. For weakly stabilizing electromigration, a cellular pattern is obtained, with a nonlinearly selected wavelength. The selection mechanism is not caused by an instability of steady-states, as suggested by previous works in the literature. Instead, the dynamics is found to exhibit coarsening *before* reaching a continuous family of stable non-equilibrium steady-states.

In non-equilibrium conditions, crystal surfaces undergo various instabilities leading to micro or nanostructures. The ultimate fate of these topographical structures is governed by the nonlinear dynamics of the surface. Understanding the nonlinear processes at play is therefore important for many applications where one wishes to design structures with a given wavelength. However, the complexity of nonlinear wavelength selection mechanisms have hindered their control, and strategies to achieve predictive design are still poorly understood. A possible strategy is to control existing instabilities by means of an external field. Here we explore the control of the faceting instability with electromigration. The faceting instability is the decomposition of a surface with a given average orientation into neighboring faceted orientations [1–5]. This instability is of thermodynamic origin, and is driven by the reduction of the surface free energy. The presence of an electric current leads to a surface electromigration mass flux  $J_E$ . This mass flux can stabilize or destabilize crystalline surfaces depending on its orientation-dependence [6–8]. Many studies have been devoted to these two instabilities. The combination of electromigration and anisotropy is already known to lead to nontrivial dynamics of voids, with the appearance of nontrivial orientations and oscillatory dynamics [9]. In this letter, we show that a faceting instability can be controlled by electromigration. In the presence of destabilizing electromigration, the faceting instability is found to be reinforced, and perpetual coarsening with a wavelength increasing as  $t^{1/2}$  is found. Strongly stabilizing electromigration supersedes the faceting instability and stabilizes the surface. This result is similar to the stabilization of the elastic stress-induced Grinfeld instability by electromigration discussed in Ref. [10]. Our most striking result appears in the presence of weakly stabilizing electromigration: we provide converging analytical and numerical evidences of the existence of a continuous branch of stable periodic steady-states. Since the dynamics exhibits a Lyapunov functional (*i.e.* an effective non-equilibrium energy functional which is decreased mono-

tonically during the dynamics), these steady-states can be characterized as *non-equilibrium meta-stable states*. Furthermore, when starting from random initial conditions, a wavelength larger than the wavelength emerging from the linear instability is selected. However, the nonlinear wavelength selection mechanism is different from the known scenarios of interrupted coarsening discussed in Refs. [11–13], or of secondary instabilities such as the Eckhaus instability [14], which all emerge from instabilities of steady-states.

*Model* – Combining previous works on faceting [4, 5] and on electromigration-induced instabilities [6–8], we write down a phenomenological nonlinear equation which governs surface dynamics. We use a one-dimensional model for the crystal surface height profile  $h(x, t)$  and slope  $\phi(x, t) = \partial_x h(x, t)$ . The average orientation  $\phi = 0$  of the surface is assumed to be unstable, and to decompose into facets of slopes  $\phi = \pm 1$ . For the sake of simplicity, we consider a Ginzburg-Landau-like orientation dependent energy:

$$\mathcal{F}[\phi] = \gamma \int dx \left[ -\frac{\phi^2}{2} + \frac{\phi^4}{4} + \frac{\epsilon^2}{2} (\partial_x \phi)^2 \right], \quad (1)$$

where  $\gamma$  is a typical surface energy scale. The last term on the r.h.s. accounts for a curvature energy cost, which regularizes facets [4, 5] at the small lengthscale  $\epsilon$ , and allows one to write down local dynamics. From Eq.(1), the local chemical potential is derived as

$$\mu = \Omega \frac{\delta \mathcal{F}[\phi]}{\delta h} = \gamma \Omega \partial_x \left[ \epsilon^2 \partial_{xx} \phi + \phi - \phi^3 \right]. \quad (2)$$

where  $\Omega$  is the atomic area. We consider surface-diffusion limited dynamics, so that chemical potential gradients induce a surface mass flux  $J_\mu = -D_L \partial_x \mu / k_B T$ , where  $k_B T$  is the thermal energy. In addition, we assume that an external electric current is applied to the crystal, leading to an orientation-dependent electromigration surface mass flux  $J_E(\phi)$ . Expanding the electromigration current for small slopes, we write  $J_E(\phi) \approx J_E(0) + \phi J'_E(0)$ . The slope-dependence of  $J_E$  may either be caused by the

anisotropy of surface diffusion [6, 15], or of the migration force [16]. As shown in Fig.1(a), electromigration is destabilizing when  $J'_E(0) > 0$ , and stabilizing when  $J'_E(0) < 0$ . This instability is the subject of a large literature, and has been the basis of the interpretation of the instabilities observed on semiconductors [17] and on metals [18]. Mass conservation reads  $\partial_t h = -\Omega \partial_x [J_\mu + J_E]$ , and leads to an evolution equation for the surface height:

$$\frac{\partial_t h}{\Omega} = D_L \frac{\Omega \gamma}{k_B T} \partial_{xx} [\epsilon^2 \partial_{xxx} h + \partial_{xx} h - \partial_x (\partial_x h)^3] - J'_E(0) \partial_{xx} h, \quad (3)$$

where we have assumed for simplicity that  $D_L$  does not depend on the orientation. Normalizing  $x$  with  $\epsilon$ ,  $t$  with  $k_B T \epsilon^4 / \Omega^2 \gamma D_L$ , and defining the dimensionless parameter  $j'_E = J'_E(0) k_B T \epsilon^2 / \Omega \gamma D_L$ , we may write a one-parameter equation for the slope:

$$\partial_t \phi = \partial_{xxxx} [\partial_{xx} \phi + \phi - \phi^3] - j'_E \partial_{xx} \phi. \quad (4)$$

The relaxation part of Eq.(4), first derived in Ref. [5], is expected to give rise to perpetual logarithmic coarsening as discussed in Ref. [19]. The electromigration part has been derived and used in many papers, see Ref. [8] for a review. When electromigration is destabilizing ( $j'_E > 0$ ), powerlaw coarsening is expected. Here, we claim that the combination of the two physical processes, faceting and electromigration, gives rise to novel dynamics.

*Linear stability analysis* – Let us start the study of Eq.(4) by means of a linear stability analysis. The growth rate  $i\omega$  of a Fourier mode  $\sim e^{i\omega t + qx}$  of wavelength  $\lambda = 2\pi/q$  reads:

$$i\omega = -q^6 + q^4 + j'_E q^2. \quad (5)$$

For  $j'_E = 0$ , all wavelengths larger than  $2\pi$  are unstable. For  $j'_E > 0$  the range of unstable wavelengths is still infinite, but extends to smaller and smaller wavelengths:  $\lambda > \lambda_+ = 2\pi/[1/2 + (1/4 + j'_E)^{1/2}]^{1/2}$ . When electromigration is weakly stabilizing  $0 > j'_E > -1/4$ , there is a finite range of unstable wavelengths  $\lambda_- < \lambda < \lambda_+$  where  $\lambda_- = 2\pi/[1/2 - (1/4 + j'_E)^{1/2}]^{1/2}$ . Finally, for strongly stabilizing electromigration, when  $j'_E < -1/4$ , the surface is linearly stable. When the surface is unstable, the wavelength  $\lambda_m = 2\pi 3^{1/2}/[1 + (1 + 3j'_E)^{1/2}]^{1/2}$  of the fastest growing mode is expected to emerge from random initial conditions (where all modes are present).

*Lyapunov functional* – The linear stability analysis predicts the existence or not of an instability from small initial perturbations. However, the amplitude of the unstable modes increases exponentially fast, and the unstable front enters into the nonlinear regime where the  $\phi^3$  term in Eq.(4) is not negligible anymore. While the analytical study of the nonlinear regime is in general delicate, the existence of an effective energy functional  $\mathcal{L}$ , sometimes called a Lyapunov functional, usually greatly

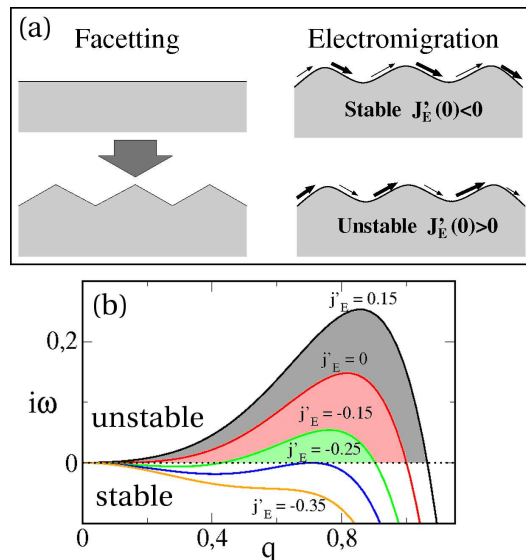


FIG. 1: Mechanism of the instability and dispersion relation: (a) Schematics of the faceting and electromigration-induced instabilities. (b) Growth rate  $i\omega$  of Fourier modes from linear stability analysis, see Eq. (5).

simplifies the analysis. Such a functional is defined as a quantity which decreases monotonously during the dynamics. The evolution equation (4) actually exhibits a Lyapunov functional (in normalized coordinates):

$$\mathcal{L}[h] = \mathcal{F}[\partial_x h] - \frac{j'_E}{2} \int dx h(x)^2. \quad (6)$$

Indeed, one may write  $\partial_t h = \partial_{xx}[\delta\mathcal{L}/\delta h]$ , leading to:

$$\partial_t \mathcal{L} = - \int dx [\partial_x (\delta\mathcal{L}/\delta h)]^2 \leq 0. \quad (7)$$

*Steady-state branches* – The space of all possible configurations for the surface profile is very large, and it is impossible to calculate the value of  $\mathcal{L}$  for all configurations. As a consequence, we would like to reduce this space to a relevant subset of shapes which is simpler to explore. A powerful approach along this line is to study the steady-states  $\phi_0(x)$ , which are the solutions of  $\partial_t \phi_0 = 0$ . Using Eq.(7), one has  $\partial_x (\delta\mathcal{L}/\delta h) = 0$ , leading to

$$\partial_{xx} [\partial_{xx} \phi_0 + \phi_0 - \phi_0^3] - j'_E \phi_0 = 0. \quad (8)$$

The central idea motivating the study of steady-states is the existence of a separation of timescales, where the shape first relaxes rapidly towards periodic steady-states. Then, these periodic solutions may exhibit an instability occurring at longer timescales, leading for example to a coarsening process [13], or to the Eckhaus instability [14].

The steady-states profiles are obtained numerically, starting with a small amplitude sinusoidal perturbation  $\sim \sin(2\pi x/\lambda)$  with one period in a box of width  $\lambda$ [23].

Following the linear stability analysis, the perturbation may grow or decay. When it grows, it reaches a finite amplitude steady-state where it stops. As shown in Fig.2 for  $j'_E > 0$ , the steady-state exhibits a monotonously increasing amplitude  $A$  as a function of the wavelength  $\lambda$ . Asymptotically for large  $A$  and  $\lambda$ , we expect the dominant term among the linear terms to be the one with the fewest derivatives, i.e.  $j'_E \phi_0$ , and this term has to balance the nonlinear term  $\partial_{xx} \phi_0^3$ , leading to  $A \sim (j'_E)^{1/2} \lambda$ . The numerical determination of the steady-state branch actually indicates that:  $A \approx 0.16(j'_E)^{1/2} \lambda$ .

When  $-1/4 < j'_E < 0$ , we obtain a bell shape branch connecting the two marginal points ( $\lambda = \lambda_-, A = 0$ ), and ( $\lambda = \lambda_+, A = 0$ ), as shown in Fig.3(a). In addition, using suitable initial conditions, we find another steady-state branch, which emerges from the primary bell-shape branch. The typical steady-state profiles are shown on Fig.3(d). Other branches could exist, and we have not tried to provide a complete analysis of all possible steady-state branches. However, and as discussed in the following, the study of the main bell-shape branch seems to be sufficient to account for the main features of the full dynamics starting from small random perturbations.

The numerical calculation of  $\mathcal{L}$  along the steady-state branches shows that  $\mathcal{L}$  decreases monotonously with  $\lambda$  for  $j'_E > 0$ , while it exhibits a minimum for  $\lambda = \lambda_{\mathcal{L}}$  when  $-1/4 < j'_E < 0$ . At this point, it is tempting to speculate that the dynamics will simply follow the gradient of  $\mathcal{L}$  along the steady-state branches [24], leading to infinite coarsening when  $j'_E > 0$  and interrupted coarsening at  $\lambda = \lambda_{\mathcal{L}}$  for  $-1/4 < j'_E < 0$ . We shall see in the following that some of these speculations are actually wrong.

*Steady-state stability* – In order to analyze the dynamics more carefully, we shall investigate the stability of steady-states with respect to small perturbations  $\phi_1(x) = \phi(x) - \phi_0(x) \ll \phi_0(x)$ . The slope variation  $\phi_1$ , leads to the following variation of  $\mathcal{L}$ :

$$\mathcal{L}_1 = \frac{1}{2} \int dx [\phi_1^2 (3\phi_0^2 - 1) + (\partial_x \phi_1)^2 - j'_E h_1^2]. \quad (9)$$

where  $\partial_x h_1 = \phi_1$ . Physically relevant steady-states must be stable with respect to perturbations with wavelengths smaller than their periodicity, and in general, we expect that the most dangerous modes are long-wavelength perturbations, as pointed out e.g. in Ref. [13]. In the long wavelength limit, where the perturbation wavelength is much larger than the periodicity of the steady-state  $\phi_0$ , one may simply replace  $\phi_0^2(x)$  by its average over one period  $\langle \phi_0^2 \rangle$ . Thus, since it has constant coefficients, Eq.(9) is now diagonal in Fourier space, and this suggests a simple stability criterion:

$$(3\langle \phi_0^2 \rangle - 1)q_1^2 + q_1^4 - j'_E > 0. \quad (10)$$

As a consequence, long wavelength modes  $q_1 \rightarrow 0$  are always unstable in the case of destabilizing electromigra-

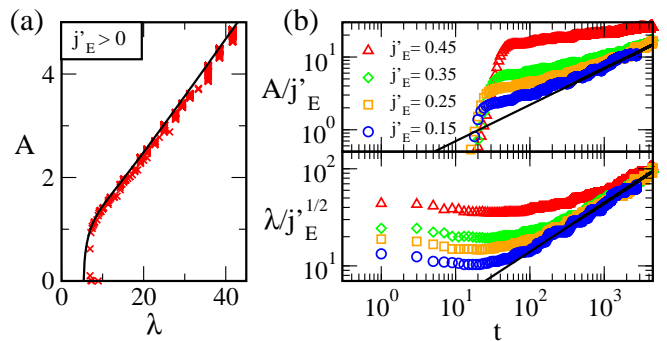


FIG. 2: *Perpetual power-law coarsening for  $j'_E > 0$* : (a) The black line indicates the steady state amplitude  $A$  versus wavelength  $\lambda$  of periodic steady-states for  $j'_E = 0.45$ . Crosses ( $\times$ ): full simulations from small random initial conditions. (b) Rescaled Amplitude  $A/j'_E$  and wavelength  $\lambda/(j'_E)^{1/2}$  as function of time for starting from small random initial conditions. The solid lines are the powerlaws discussed in the text.

tion  $j'_E > 0$ . This is in agreement with the above speculation of perpetual coarsening. In addition, we may also gain information about the coarsening exponent. Indeed, at long wavelengths we have  $\mathcal{L}_1 \approx -\int dx j'_E h_1^2/2$ , and as a consequence one has  $\partial_t h_1 \approx -j'_E \partial_{xx} h_1$ . This relation provides a link between lengthscales  $x$ , assumed to be  $\sim \lambda$ , and timescales  $t$ , leading to  $\lambda \sim (j'_E)^{1/2} t^{1/2}$ . Using the previously derived linear relation between  $\lambda$  and  $A$ , we also find  $A \sim j'_E t^{1/2}$ .

When  $-1/4 < j'_E < 0$ , from Eq.(10), the steady-states should be stable for all  $q_1$  when

$$\langle \phi_0^2 \rangle > \frac{1}{3} [1 - 2(-j'_E)^{1/2}]. \quad (11)$$

This criterion indicates that the upper part of the branch between the green stars in Fig.3(a,b) should be stable, while the lower parts close to  $\lambda_{\pm}$  should be unstable [25]. Such a result suggests that the system is stuck once the dynamics hits the stable part of the steady-state branch, and as a consequence, it cannot evolve towards the minimum of  $\mathcal{L}$  at  $\lambda = \lambda_{\mathcal{L}}$ .

*Full dynamics* – These results are confirmed by the full numerical solution of Eq.(4) starting from small random perturbations of a flat state in a system of size  $L = 500$ . The results are shown in Fig.4. First, and as expected, we find stable dynamics for  $j'_E < -1/4$ .

For destabilizing electromigration  $j'_E > 0$ , perpetual coarsening is found, as shown on Fig.4(a), and after a transient related to the linear instability, the dynamics follows the steady-state branch in the  $(\lambda, A)$  plane, as shown in Fig.2(a). We also confirm the scaling laws given above in Fig.2(b), and find the prefactors:  $\lambda \approx 1.4(j'_E)^{1/2} t^{1/2}$ , and  $A \approx 0.22 j'_E t^{1/2}$ . The ratio of these prefactors is in perfect agreement with the asymptotic behavior of the steady-states discussed above  $A \approx 0.16(j'_E)^{1/2} \lambda$ .

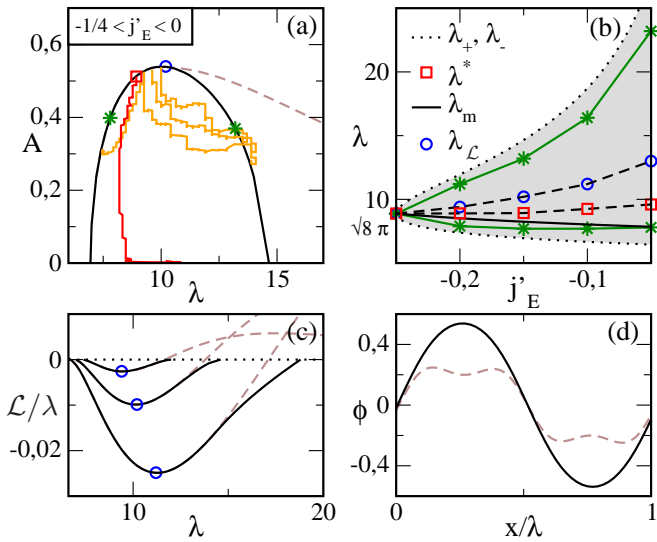


FIG. 3: *Nonlinear wavelength selection for  $-1/4 < j'_E < 0$ :* (a) The (black) solid and (brown) dashed lines indicate the steady state amplitude  $A$  versus wavelength  $\lambda$  for  $j'_E = -0.15$ . Red line: full dynamics from small random initial conditions in an extended system. Orange lines: dynamics starting from slightly perturbed periodic steady-state in an extended system. Green stars indicate theoretical limit of stability of the steady-state branch. (b) The shaded region corresponds to the linearly unstable region. Green stars: limits of steady-state stability. (c) Lyapunov functional density  $\mathcal{L}/\lambda$  evaluated from the steady state profiles. (d) Steady state profiles numerically obtained for the two branches at  $j'_E = -0.15$ .

For weakly stabilizing electromigration  $-1/4 < j'_E < 0$ , the dynamics starts with a rapid increase of the amplitude due to the linear instability. Then, the average wavelength increases *before* the dynamics hits the steady-state branch at  $\lambda = \lambda^*$ , as shown in Fig.3(a). When the dynamics reaches the steady-state branch, it stops, as expected from the above prediction of steady-state stability. As a consequence, the system never reaches the minimum of  $\mathcal{L}$  along the steady-state branch.

In order to check further the stability of the steady-state branch, we have performed simulations in boxes of width around 80 periods starting with periodic steady-states with small perturbations. These simulations confirm the stability of the upper part of the branch, and the instability of the lower part, in quantitative agreement with the condition (11). As seen in Fig.3(a), the instability does not lead to a trajectory of the system along the steady-state branch in the  $(\lambda, A)$  plane. Instead, the trajectory escapes from the branch and returns to it, stopping in the same region as the dynamics from flat initial conditions. Fig.3(b) summarizes the evolution of the different lengthscales as a function of  $j'_E$ .

*Conclusions and perspectives* – In summary, we have studied the control of the faceting instability by means of electromigration. For strong stabilizing electromigration,

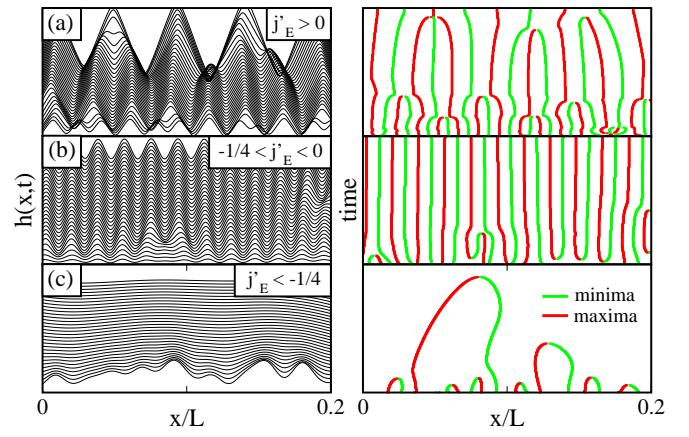


FIG. 4: *Full dynamics and coarsening:* Left: surface height  $h(x,t)$  as a function of space for different times in the three different regimes: (a)  $j'_E = 0.45$ , (b)  $j'_E = -0.15$ , (c)  $j'_E = -0.3$ . Right: Corresponding spatiotemporal portrait of the extrema of the height profile.

the surface is stable. Under weakly stabilizing electromigration, the surface exhibits a periodic cellular structure with a nonlinearly selected wavelength. When electromigration is destabilizing, perpetual coarsening is found with a coarsening exponent  $1/2$ .

In the case of weakly stabilizing electromigration, we find a continuous family of stable periodic steady-states. These states can be interpreted as non-equilibrium metastable states, where metastability is here defined as local stability with respect to a non-equilibrium Lyapunov functional playing the role of an effective energy.

In the literature, several cases of nonlinear wavelength selection on crystal surfaces have been interpreted as interrupted coarsening, such as for mound growth [11], atomic step meandering [12], and ion sputtering [20]. However, the nonlinear wavelength selection scenario presented in this Letter does not correspond to interrupted coarsening, as defined e.g. in Ref. [13], or to another instability of steady-states, such as in the Eckhaus instability [14]. Indeed, we only observe a small amount of coarsening *before* the dynamics hits the steady-state branch. Once the system has reached a steady-state, it is stable and the evolution stops.

These results may provide hints to understand other nonlinear wavelength selection scenarios obtained in the literature, such as in the combination of growth and faceting as discussed in Ref. [21, 22] (where nonlinear wavelength selection occurs between a coarsening regime, and a chaotic regime). More generally, we hope that our work will provide milestones towards the novel methods to control the size of nano-structures emerging from surface morphological instabilities.

KM was supported by the Marie Curie FP7-PEOPLE-2009-IEF program.

- 
- [1] A. Chame, S. Rousset, H. Bonzel, and J. Villain, *Bulg. Chem. Commun.* **29**, 398 (1996).
- [2] Y. Kim, M. H. Jo, T. C. Kim, C. W. Yang, J. W. Kim, J. S. Hwang, D. Y. Noh, N. D. Kim, and J. W. Chung, *Phys. Rev. Lett.* **102**, 156103 (2009), URL <http://link.aps.org/doi/10.1103/PhysRevLett.102.156103>.
- [3] H.-C. Jeong and J. D. Weeks, *Phys. Rev. Lett.* **75**, 4456 (1995), URL <http://link.aps.org/doi/10.1103/PhysRevLett.75.4456>.
- [4] A. Di Carlo, M. Gurtin, and P. Podio-Guidugli, *SIAM J. Appl. Math.* **52**, 1111 (1992).
- [5] F. Liu and H. Metiu, *Phys. Rev. B* **48**, 5808 (1993), URL <http://link.aps.org/doi/10.1103/PhysRevB.48.5808>.
- [6] J. Krug and H. T. Dobbs, *Phys. Rev. Lett.* **73**, 1947 (1994), URL <http://link.aps.org/doi/10.1103/PhysRevLett.73.1947>.
- [7] J. Chang, O. Pierre-Louis, and C. Misbah, *Phys. Rev. Lett.* **96**, 195901 (2006), URL <http://link.aps.org/doi/10.1103/PhysRevLett.96.195901>.
- [8] C. Misbah, O. Pierre-Louis, and Y. Saito, *Rev. Mod. Phys.* **82**, 981 (2010), URL <http://link.aps.org/doi/10.1103/RevModPhys.82.981>.
- [9] P. Kuhn, J. Krug, F. Hausser, and A. Voigt, *Phys. Rev. Lett.* **94**, 166105 (2005), URL <http://link.aps.org/doi/10.1103/PhysRevLett.94.166105>.
- [10] V. Tomar, M. R. Gungor, and D. Maroudas, *Phys. Rev. B* **81**, 054111 (2010), URL <http://link.aps.org/doi/10.1103/PhysRevB.81.054111>.
- [11] P. Politi and J. Villain, *Phys. Rev. B* **54**, 5114 (1996), URL <http://link.aps.org/doi/10.1103/PhysRevB.54.5114>.
- [12] G. Danker, O. Pierre-Louis, K. Kassner, and C. Misbah, *Phys. Rev. E* **68**, 020601 (2003), URL <http://link.aps.org/doi/10.1103/PhysRevE.68.020601>.
- [13] P. Politi and C. Misbah, *Phys. Rev. Lett.* **92**, 090601 (2004), URL <http://link.aps.org/doi/10.1103/PhysRevLett.92.090601>.
- [14] W. Eckhaus, *Studies in Nonlinear Stability Theory* (Springer, Berlin, 1965).
- [15] S. Stoyanov, *Jpn. J. Appl. Phys.* **29**, L659 (1990).
- [16] O. Pierre-Louis, *Phys. Rev. Lett.* **96**, 135901 (2006), URL <http://link.aps.org/doi/10.1103/PhysRevLett.96.135901>.
- [17] A. Latyshev, A. Aseev, A. Krasilnikov, and S. Stenin, *Surface Science* **213**, 157 (1989), ISSN 0039-6028, URL <http://www.sciencedirect.com/science/article/pii/0039602889>.
- [18] R. P. Johnson, *Phys. Rev.* **54**, 459 (1938), URL <http://link.aps.org/doi/10.1103/PhysRev.54.459>.
- [19] F. Hauber and A. Voigt, *Phys. Rev. E* **79**, 011115 (2009), URL <http://link.aps.org/doi/10.1103/PhysRevE.79.011115>.
- [20] J. Muñoz García, R. Gago, L. Vázquez, J. A. Sánchez-García, and R. Cuerno, *Phys. Rev. Lett.* **104**, 026101 (2010), URL <http://link.aps.org/doi/10.1103/PhysRevLett.104.026101>.
- [21] A. A. Golovin, A. A. Nepomnyashchy, S. H. Davis, and M. A. Zaks, *Phys. Rev. Lett.* **86**, 1550 (2001), URL <http://link.aps.org/doi/10.1103/PhysRevLett.86.1550>.
- [22] T. V. Savina, A. A. Golovin, S. H. Davis, A. A. Nepomnyashchy, and P. W. Voorhees, *Phys. Rev. E* **67**, 021606 (2003), URL <http://link.aps.org/doi/10.1103/PhysRevE.67.021606>.
- [23] We use an finite difference explicit scheme.
- [24] More precisely, since  $\lambda$  varies, we calculate the density  $\mathcal{L}/\lambda$ .
- [25] Due to numerical difficulties in the calculation of the steady-state branch for  $\lambda$  close to  $\lambda_+$  when  $0 > j'_E \geq -0.1$ , the upper stability limit in Fig.3(b) was obtained from an interpolation for  $j'_E = -0.1, -0.05$ .